ESC European Society of Cardiology

European Heart Journal Open (2025) **5**, oeae106
https://doi.org/10.1093/ehjopen/oeae106

ORIGINAL ARTICLE
Valvular heart disease

Characterization of LTBP2 mutation causing mitral valve prolapse

Shoshi Shpitzen[1,*], Haim Rosen[2], Ayal Ben-Zvi[3], Karen Meir[4], Galina Levin[5], Amichay Gudgold[1], Shifra Ben Dor[6], Rebecca Haffner[7], Donna R. Zwas[5], David Leibowitz[5], Susan A. Slaugenhaupt[8], Eyal Banin[9], Rotem Mizrachi[9], Alexey Obolensky[9], Robert A. Levine[10], Dan Gilon[5], Eran Leitersdorf[1], Idit Tessler[1,11,12], Noga Reshef[1], and Ronen Durst[1,5,*]

[1]Department of Medicine, Cardiovascular Precision Medicine Center, Hadassah Hebrew University Medical Center, P.O. Box 12000, 9112001 Jerusalem, Israel; [2]The Kuvin Center for the Study of Infectious and Tropical Diseases, Institute for Medical Research-Israel-Canada, Hebrew University—Hadassah Medical School, 9112001 Jerusalem, Israel; [3]Developmental Biology and Cancer Research, Hadassah—Hebrew University Medical School, 9112001 Jerusalem, Israel; [4]Department of Pathology, Hadassah Hebrew University Medical Center, P.O. Box 12000, 9112001 Jerusalem, Israel; [5]Department of Cardiology, Hadassah Hebrew University Medical Center, P.O. Box 12000, 9112001 Jerusalem, Israel; [6]Department of Life Sciences Core Facilities, Weizmann Institute of Science, Herzl St 234, 7610001 Rehovot, Israel; [7]Department of Veterinary Resources, Weizmann Institute of Science, Herzl St 234, 7610001 Rehovot, Israel; [8]Center for Genomic Medicine, Massachusetts General Hospital Research Institute, 185 Cambridge Street, Boston, MA 02114, USA; [9]Center for Retinal and Macular Degenerations, Department of Ophthalmology, Hadassah Hebrew University Medical Center, P.O. Box 12000, 911200120 Jerusalem, Israel; [10]Cardiac Ultrasound Laboratory, Massachusetts General Hospital, Harvard Medical School, 185 Cambridge Street, Boston, MA 02114, USA; [11]Sheba Medical Center, Ramat Gan, P.O. Box 12000, 911200120 Jerusalem, Israel; and [12]Faculty of Medicine, Tel-Aviv University, P.O. Box 12000, 911200120 Tel-Aviv, Israel

Received 19 September 2024; revised 14 October 2024; accepted 17 December 2024; online publish-ahead-of-print 3 January 2025

Handling Editor: Patrizio Lancellotti

Aims Mitral valve prolapse (MVP) is a common valvular disorder associated with significant morbidity and mortality, with a strong genetic basis. This study aimed to identify a mutation in a family with MVP and to characterize the valve phenotype in LTBP2 knockout (KO) mice.

Methods and results Exome sequencing and segregation analysis were performed on a large family with MVP. Two mouse strains were generated: a complete KO of the *LTBP2* gene and a knockin (KI) of the human mutation. At 6 months, phenotyping was conducted using echocardiography, histology, eye optical coherence tomography, and quantitative polymerase chain reaction analysis for TGF-β signalling targets (periostin/*POSTN*, *RUNX2*, and *CTGF*) in valve tissues. *LTBP2* rs117800773 V1506M mutation exhibited segregation with MVP. *LTBP2* KO mice had a higher incidence of myxomatous changes by histology (7 of 9 of KO vs. 0 of 7 control animals, $P = 0.00186$) and echocardiography (7 of 9 vs. 0 of 8, $P = 0.0011$). *LTBP2* KI mice for the human mutation showed a significantly elevated myxomatous histological phenotype (8 of 8 vs. 0 of 9, $P = 0.00004$) as well as by echocardiography (6 of 8 vs. 0 of 9, $P = 0.00123$). Knockout mice demonstrated an increase in the depth of the anterior chamber as well as reduced visual acuity. *LTBP2* KO mice demonstrated overexpression of both TGF-β signalling targets *RUNX2* and periostin ($P = 0.0144$ and $P = 0.001826$, respectively).

Conclusion We report a KO mouse strain with an *LTBP2* mutation, demonstrating a valve phenotype, alongside a family with a novel mutation linked to MVP.

* Corresponding author. Tel: +97226778019, Email: Shpi@hadassah.org.il (Sh.S.); Tel: +97226778019, Email: Durst@hadassah.org.il ronen.durst@mail.huji.ac.il (R.D.)

Graphical abstract

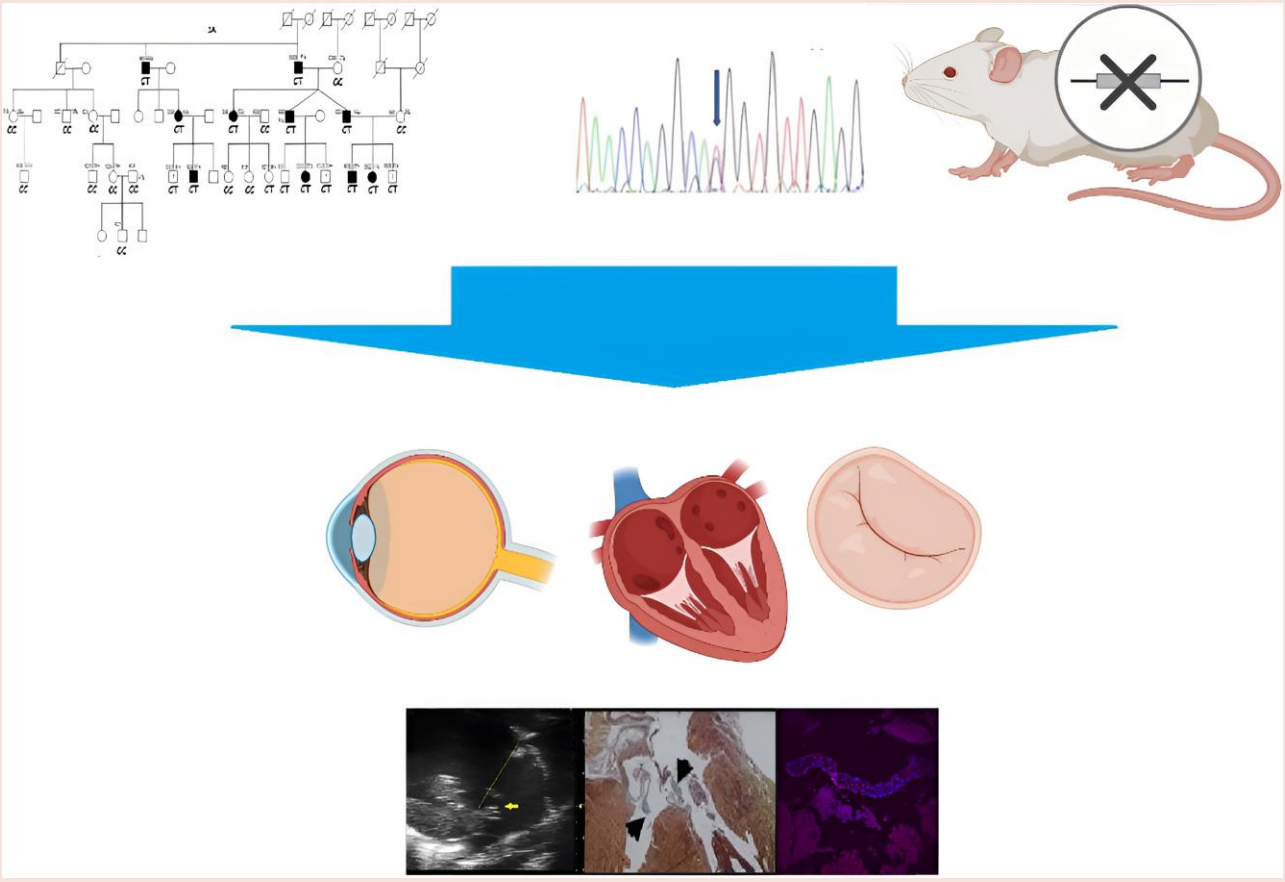

Keywords Mitral valve prolapse • LTBP2 • Myxomatous valve

Introduction

Mitral valve prolapse (MVP) is a very common cardiac valvular disorder that occurs in 2.4% of the general population.[1] Mitral valve prolapse is characterized by the displacement of one or both leaflets towards the left atrium during valvular closure during systole.[2–4] Myxomatous alteration in the valvular tissue, changes in collagen organization, and an increase in glycosaminoglycans lead to biomechanically inferior valvular tissue that results in prolapse of the mitral leaflets into the left atrium.[3,4] Prolapse of the leaflets may cause progressive degeneration and leakage, and therefore, MVP is a leading indication for mitral valve surgery.[5] Mitral valve prolapse can be complicated by infective endocarditis, valvular regurgitation, and congestive heart failure. In addition, several recent studies have demonstrated an association between MVP and ventricular arrhythmias and sudden cardiac death.[6–8] Dysregulation of the extracellular matrix (ECM) components plays a key role in mediating these changes and is essential for understanding the genetic pathways causing the disease.[9]

Mitral valve prolapse is classified as non-syndromic or syndromic. Non-syndromic MVP can be familial or sporadic. Syndromic MVP occurs in association with connective tissue disorders such as Marfan syndrome (MFS), Loeys–Dietz syndrome, Ehlers–Danlos syndrome, osteogenesis imperfecta, pseudoxanthoma elasticum, and aneurysm–osteoarthritis syndrome.[2] Familial studies of idiopathic or non-syndromic MVP suggest an autosomal dominant model of inheritance with age-dependent incomplete penetrance.[1–4]

A prior genome-wide association study (GWAS) suggested an association between *LTBP2* (Latent Transforming Growth Factor Beta Binding Protein 2) and MVP.[10] *LTBP2* is a member of the larger *LTBP* family, proteins that are expressed in the ECM thought to have role in maintaining ECM functional and structural integrity. More recently, LTBP2 plasma levels were associated with worse outcome in patients with dilated cardiomyopathy.[11] To confirm the causative role of *LTBP2*, we created two strains of mouse models, an *LTBP2* knockout (KO) model with a gene KO and an *LTBP2* knockin (KI) model of the rs117800773 V1506M mutation that was found in a large pedigree segregating the trait. Both strains demonstrated high prevalence of MVP on echocardiogram and histology analyses.

Methods

Genetic analysis

The study was approved by the Hadassah Hebrew University Hospital in Jerusalem IRB and the Israeli Ministry of Health Committee for Genetic Studies (0464-10-HMO). All participants consented to participate in the

study. After signing an informed consent, subjects were clinically phenotyped by transthoracic echocardiography using a standard imaging protocol.[1,2,12] Mitral valve prolapse was defined by echo as leaflet displacement of at least 2 mm above the mitral annular line on the parasternal long-axis view (*Figure 1*).[13] DNA was extracted from peripheral blood leucocytes using the salting-out method. Exome sequencing was done on an Illumina platform, with a mean coverage of >150X. Bioinformatics was performed using the TGex NGS analysis platform.[14] The analysis platform was used for extraction of raw sequencing data from the sequencing provider, followed by primary and secondary pipelines to generate variant call format (VCF) files with exome variants. Variant call format files went through a comprehensive annotation pipeline for analysis, and all the resulting annotated variants were displayed in an interactive user interface for analysis interpretation and selection of plausible candidates in the context of MVP and related keywords. The annotation pipeline, as well as the annotation database and architecture of a variant interpretation of the platform, has been described in detail elsewhere.[14] Briefly, the analysis is based on the standard steps of basic variant annotation, allele frequency databases, and variant damage prediction and offers phenotype-driven interpretation that relies on a comprehensive knowledge base and annotation of structural variants. The genes were validated by polymerase chain reaction (PCR) and Sanger sequencing.

Animal model

gRNA design and the generation of *LTBP2* knockout/knockin mice

All mice experiments were approved by the IACUC committees of the Weizmann Institute and the Hebrew University Medical Center (MD-21-16445-3) and were carried out in accordance with their approved guidelines. gRNAs were designed using a combination of *in silico* design tools, including the MIT CRISPR design tool[15] and sgRNA Designer, Rule Set 2,[16] in the Benchling implementations[17] SSC[18] and CRISPOR.[19]

Two gRNAs were designed to target the *LTBP2* region, *LTBP2* upstream guide (5′-TTT GGC ACC GAG AAG CGA GC-3′) and *LTBP2* downstream guide (5′-AAT CGG TTG TGG CAC CCC GT-3′), respectively, to create genetic KO of *LTBP2*. The planned deletion of 551 bp removes the beginning of the gene, including part of the promoter, the transcription start site, and the initiator methionine. We also designed a guide (5′-CGA TGC CTC AAC ATA GTG CC-3′) and an ssODN repair template (TCCCGAAGATGCC GATGAATGTGTACTGTTTGGGCCTGCTCTCTGCCAGAATGGCCG ATGTCTGAATATTATGCCTGGATACATATGCCTGTGCAACCCTGG CTACCACTATGATGCCTCCAGCAGGAAGTGCCAGGGTGAGGAC) to phenocopy the human mutation rs117800773 V1506M, corresponding to V1471M in the mouse (see Supplementary material online, *Figure S2*). Cas9 nuclease, crRNA, tracrRNAs, and ssODN were purchased from Integrated DNA Technologies. *LTBP2* mice were generated at the Transgenic Facility at the Weizmann Institute of Science using CRISPR/Cas9 genome editing in isolated one-cell mouse embryos as described.[20] C57Bl/6JOlaHsd mice were purchased from Envigo, Israel, and maintained in specific pathogen-free conditions. Mice were maintained on a 12 h light/dark cycle, and food and water were provided *ad libitum*. Cas9-gRNA ribonucleoprotein complexes were delivered to one-cell embryos via electroporation using the Bio-Rad Gene Pulser (Bio-Rad, Hercules, CA, USA). Electroporated embryos were transferred into the oviducts of pseudo-pregnant ICR females (Envigo, Israel). Genomic DNA from F0 pups was analysed at weaning for the 551 bp deletion and the V1506M mutation by PCR and Sanger sequencing. The pups were genotyped by PCR (PCRbio HS Taq mix) and Sanger sequencing.

The validation of KO and KI were done by using PCR with the following primers:

- LTBP2 (KO) F 5′-GTT TGC CCA GGA CAG GAA AA-3′
- LTBP2 (KO) R 5′-GTT CCA CTC AGA GGG CGA-3′
- LTBP2 3F (KI) 5′-TCC TCC CGA AGA TGC CGA-3′
- LTBP2 3R (KI) 5′-CGT TCT CAC AGG CCA AGT CC-3′

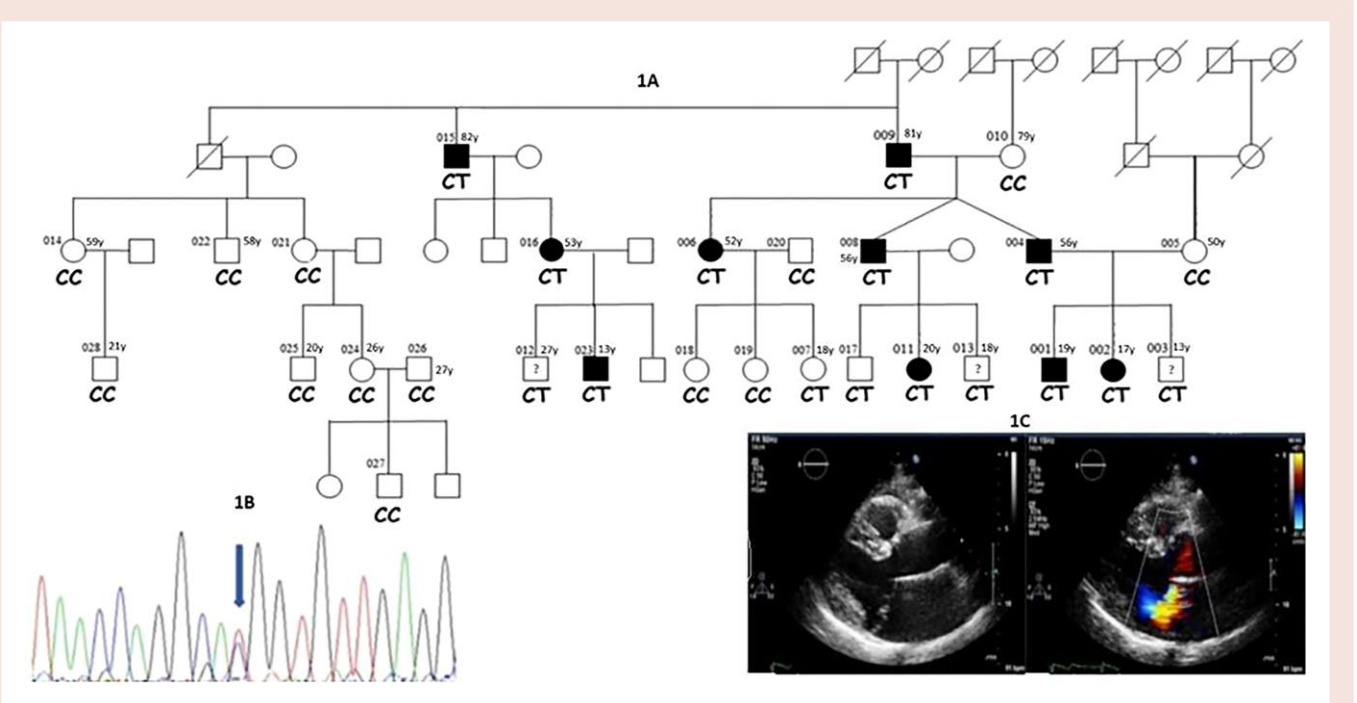

Figure 1 (*A*) Pedigree demonstrating LTBP2 V1506M mutation. Segregation with mitral valve prolapse in the pedigree. Dark shapes are mitral valve prolapse, and empty shapes are normal phenotype. A question mark denotes either equivocal phenotype or that an echocardiogram was not available. *LTBP2* genotype is at the bottom: CC is the wild-type allele and CT heterozygote for the V1506M mutation. The left top number is a serial number for the individual in the family. The right top number when available is the age of phenotyping. (*B*) The sequence variation with a blue arrow pointing to the mutation. (*C*) A demonstrative parasternal long axis with and without colour Doppler of individual 004, demonstrating mitral valve prolapse and significant regurgitation.

Western blot analysis

To validate the reduction in *LTBP2* protein in the KO mice, total protein was purified from the whole heart using homogenization in T-PER buffer (Tissue Protein Extraction Reagent, Thermo Fisher Scientific) and protease inhibitor (Pierce Protease Inhibitor Tablets A32953, Thermo Fisher Scientific) analysed by 4–12% SDS–PAGE (Thermo Fisher Scientific) and immunoblotting with *LTBP2* antibody 1:100 [*LTBP2* (E-10) SC-166199] and goat anti-mouse as a secondary antibody 1:10 000 (Jackson ImmunoResearch Laboratories cat: 115035166) (see Supplementary material online, *Figure S1*).

Animal echocardiography

Echocardiography was performed at 6 months of age. This was chosen based on preliminary data that the phenotype is fully expressed by this age. Both the pathologist and the cardiologist performing the echocardiography were blinded to the underlying genotype. The echocardiographers (D.G., R.A.L., and R.D.) are fully trained in both human and mice echo performance and reading. Echocardiography was performed using the Vevo3100 Lazer-x Ultrasound (Visual Sonic Ltd, London, UK) at The Wohl Institute for Translational Medicine at the Hadassah Hebrew University Medical Center. After sedation with isoflurane, the animals were placed in the prone position. A parasternal long-axis view was obtained. Displacement of the posterior leaflet was confirmed if the leaflet traversed the annular line drawn between the hinge points of the anterior and posterior leaflets. Other parameters that are related to MVP, such as anterior displacement of the coaptation line, were used to confirm the phenotype.[21,22]

Histological analysis

LTBP2 KO and KI mice were sacrificed for histopathologic analysis at 6 months. Mitral valve disease lesion was examined using the murine model of both strains of *LTBP2*. For histopathological analysis, hearts were processed in 4% formaldehyde. Paraffin-embedded tissue slices included left ventricular apex, mitral valve, and the aortic valve. Thin slices of the hearts were prepared using microtome and placed for haematoxylin and eosin staining (H&E) staining and Movat pentachrome staining. Movat's stain (Movat Pentachrome Stain Kit ab245884) is a pentachrome stain that highlights the various constituents of connective tissue and H&E. It differentiates collagen, elastic, muscle, mucin, and fibrin by colour (muscle in red, glycosaminoglycan in blue, elastin in dark purple, nuclei in black, and collagen in yellow).

Immunofluorescence staining for *LTBP2*-deficient valve tissue

LTBP2 KO and wild-type (WT) mice were sacrificed at 6 months by cervical dislocation. Hearts were processed in 4% formaldehyde. Paraffin-embedded tissue sectioned at 4 μm thickness included the left ventricular apex and mitral valve. Slides were deparaffinized in xylene and dehydrated through a graded ethanol series. The slides were then transferred to a pressure cooker in 10 mM citrate buffer pH 6.0 (Antigen Unmasking Solution, citric acid-based vector H-3300) for antigen retrieval. Blocking section was done in CaseBlock 10 (Abcam AB64226) for 10 min and incubated with *LTBP2* antibodies 1:200 (kind gift of Dr Gerthad Sengle from the Center for Molecular Medicine Cologne, Germany) overnight at 4°C. Alexa Fluor conjugated 647 donkey anti rabbit 1:200 (Jackson ImmunoResearch 711605152) was used as a secondary antibody for 45 min at room temperature. The section was mounted with DAPI mounting (DAPI Fluoromount-G, Southern Biotech 0100-20) and covered with a coverslip. The sections were observed, and images were taken with a confocal fluorescence microscope (Nikon Spinning Disk Microscope, Yokogawa W1 Spinning Disk, 2 SCMOS ZYLA cameras ×40 objective, 200 msc exposure). The processing was done by NIS-Elements software package for multidimensional experiments, with JOBS for high content acquisition and analysis, deconvolution, tracking, and 3D automatic measurements. Elastin immunostaining was done similarly with similar tissue preparation and imaging process. Elastin antibodies 1:100 (Bioss Antibodies bs-1756R) were used with an overnight incubation at 4°C. Alexa Fluor conjugated 647 donkey anti rabbit 1:200 (Jackson ImmunoResearch 711605152) was used as a secondary antibody as above.

Quantitative polymerase chain reaction

After sacrifice, hearts were preserved on ice-cold saline solution. The hearts were dissected under a binocular from the aorta to the apex. Mitral valve tissue was identified and excised. Total RNA was extracted from the heart valve using Tri reagent (Sigma T9424) according to the manufacturer's protocol. For reverse transcription reaction, we used Quantabio kit (qScript cDNA Synthesis Kit 95047-100, Quantabio, Beverly, MA, USA), and real-time quantitative reverse transcription PCR was done on three genes: mouse *RUNX2*, mouse Periostin, and mouse CTGF using Syber Green FastMix (Quantabio 66185483). Rodent GAPDH was used as the standard. Primers for the reactions were as follows: *RUNX2* F 5′-AGA GCC AGG CAG GTG CTT C-3′, *RUNX2* R 5′-TCT CAG TGA GGG ATG AAA TGC T-3′, Periostin F 5′-CCA CAG GAG GTG GAG AAA CA-3′, Periostin R 5′-GAT CGT CTT CTA GGC CCT TGA-3′, CTGF F 5′-GGA GTG TGC ACT GCC AAA GA-3′, and CTGF R 5′-ACT CAC CGC TGC GGT ACA C-3′. The samples were analysed on ABI-7300 Real Time PCR System (Applied Biosystems, Waltham, MA, USA).

Mice eye analysis

Visual acuity

Visual acuity (VA) of WT and *LTBP2* KO mice was evaluated using the optomotor response test (OptoMotry, CerebralMechanics, Lethbridge, AB, Canada), as previously described.[23] Animals were placed on a small platform at the centre of a virtual drum presented by four liquid crystal display panels. After a short adaptation period, VA was measured at 100% contrast by recording the tracking response to a rotating visual stimulus.

In vivo imaging

Anterior chamber structure was studied *in vivo* using single horizontal 15° optical coherence tomography (OCT) b-scans passing through the centre of the cornea (SPECTRALIS, Heidelberg). The procedures were performed in anaesthetized animals [intraperitoneal injections of a mixture of 0.85 μL ketamine (Bedford Laboratories, Bedford, OH, USA) and 0.15 μL xylazine (VMD, Arendonk, Belgium) with dilated pupils (cyclopentolate 1% applied twice, Laboratorio Edol, Carnaxide, Portugal, and tropicamide 1% applied once; Fisher Pharmaceuticals, Tel-Aviv, Israel).

The anterior chamber depth (ACD, between corneal endothelium and anterior capsule of the lens), iridocorneal angle, and pupil diameter were measured using Image-Pro Plus 6.0 software.

Eye histology

Eyes were enucleated, fixed in Davidson solution, embedded in Paraplast, and sectioned at 5 μm thickness through the centre of the optic nerve. For descriptive histology, sections were stained with H&E. All observations, photography, and processing were performed using the Aperio CS2 slide scanner and ImageScope software.

Statistical analyses

Comparison between categorical parameters was made by the χ^2 test; *P*-values of each quantitative polymerase chain reaction experiment were repeated three times for each set of RNA mitral valve, and results were pooled for statistical analysis. Student's two-tailed *t*-test was used for comparison between two groups. Movat's pentachrome and echocardiogram analyses were made by χ^2 test. Eye imaging parameters were tested using a two-tailed Student's *t*-test.

Results

We studied 4 generations of a Jewish Ashkenazi family comprising 28 individuals. The family had a severe clinical phenotype of MVP as several developed severe valvular disease requiring valve repair surgery (*Figure 1*) (*Table 1* provides echocardiographic and genetic data of the family). The family lacks extra cardiac connective tissue features, and all do not fulfil any of the criteria for connective tissue disorders.[24–26] The severity of mitral regurgitation (MR) was more noticeable among middle-aged individuals within the family. Three middle-aged individuals had valve surgery

Table 1 Echocardiographic and genetic data on the pedigree participants

Sample no.: MVP	Genotype	DOB	MVP	LA (cm)	LV (cm)	Aorta diameter	MR
1	CT	18	Positive	3.3	4.76	2.7	Mild
2	CT	16	Positive	3.1	4.2	2.4	Mild
4	CT	55	Positive	3.26	5.1	3.5	Severe
6	CT	51	Positive	3.2	4.8	2.9	Moderate
8	CT	55	Positive	4.4	5.3	3.3	Severe
10	CC	78	Negative	3.9	2.4	2.9	Mild
11	CT	19	Positive	2.9	4.6	2.7	Moderate
12	CT	26	Borderline	3.4	5.02	3.4	
13	CT	17	Negative	3.4	5.3	3	
14	CC	18	Negative	3.1	4.3	3.3	Mild
15	CT	81	Positive	4.6	5.8	3.7	Severe
16	CT	52	Positive	3.8	5.2	3.2	Mild
17	CT	25	Negative	4.2	5.2	3.1	
18	CC		Negative	2.9	4.3	2.6	
19	CC	25	Negative	3.6	4.7	2.4	Mild
22	CC	57	Negative	3.7	4.9	3.6	Mild

(#004, #008, and #009). In contrast, younger members displayed a milder form of MVP with non-significant MR. Of note, there were several patients with mitral annular disjunction (for example, individuals 4, 8, and 15). There was no recorded clinically significant ventricular arrhythmia or sudden death in the family. Four family members (#004, #008, #009, and #011) were screened for a shared mutation by exome sequencing. Three hundred and sixty-one variants in 279 genes were found. Among these, pathogenic autosomal dominant mutations were identified in 11 genes (*Table 2*). None of the known connective tissue genes was mutated. These were tested for segregation with the trait in the entire family.

Only the *LTBP2* rs117800773 V1506M[27] (chr14:74970695) mutation showed segregation with trait (*Figure 1*). rs117800773 V1506M is a rare mutation [minor allele frequency of 0.001 in Europeans (https://www.ncbi.nlm.nih.gov/clinvar/variation/314272/?oq=rs117800773&m=NM_000428.3(LTBP2):c.4516G%3EA%20(p.Val1506Met)]. The *LTBP2* gene was a leading candidate as it was also found to be positively associated with MVP on a recent large GWAS,[10] supporting our finding. In addition, *LTBP2* is associated with TGFβ signalling activity, which has been shown to be disrupted in mitral valvulopathy in the setting of Marfan's syndrome.[28]

As these data supported the hypothesis that an *LTBP2* mutation led to myxomatous degeneration in both a family and a GWAS study, the next step was to investigate whether *LTBP2* mutation in this gene can cause myxomatous degeneration in mice. We therefore established two lines of mice using CRISPR/Cas9 technology, one with a major deletion (551 bp) at the 5′ end of the gene, including part of the promoter, the transcription start site, and the initiator methionine resulting in complete KO of the gene and the other, a KI of the rs117800773 V1506M mutation strain. The mouse strains were verified by PCR followed by Sanger sequencing and by western blot analysis, using an *LTBP2*-specific antibody (see Supplementary material online, *Figures S1* and *S2*).

Exploring the knockout and knockin phenotypes by both functional imaging (echocardiogram) and structural by histological examination

Whole heart extracts were used for western blot analysis of *LTBP2*. Knockout animals lacked *LTBP2* protein expression in heart tissue

Table 2 Next-generation sequencing analysis was performed on four affected family members and reveals all the genes that have been associated with the clinical data and reasonable functional influence on the protein structure

Gene	Mutation location	Substitution
ACAD9	chr3:128622922	G > A
ACADL	chr2:211085491	G > A
AOAH	chr7:36552787	A > AG
ATN1	chr12:7045892	C > CAGT
CDRT4	chr17:15343528	CT > C
GSN	chr9:124088908	C > G
LTBP2	chr14:74970695	C > T
MYOC	chr1:171607791	G > A
NUBPL	chr14:32295912	C > T
SYNE1	chr6:152472789	G > A
PGPEP1L	chr15:99511805	CT > C

All the family members were tested for segregation and only *LTBP2* V1506M mutation segregated with mitral valve prolapse in the extended family pedigree.

(see *Figure 2*, *Table 3* and Supplementary material online, *Figure S1*). The leaflets of KO mice did not exhibit *LTBP2* in immunofluorescence staining (*Figure 2G* and *H*).

Histology

Movat's pentachrome staining and H&E demonstrated structural expansion of the valvular ECM, as well as thickening and myxomatous degeneration (*Figure 2*). Knockout mice demonstrated a significantly higher rate of myxomatous changes by histology [7 of 9 of the affected mice vs. 0 of 7 control animals ($P < 0.00186$)]. Knockin mice demonstrated a significantly higher phenotype rate by histology [8 of 8 vs. 0 of 9 ($P < 0.00004$)] (*Figure 2A–D* and *Table 3*). Both KO and KI demonstrated increased leaflet area by planimetry of these histological

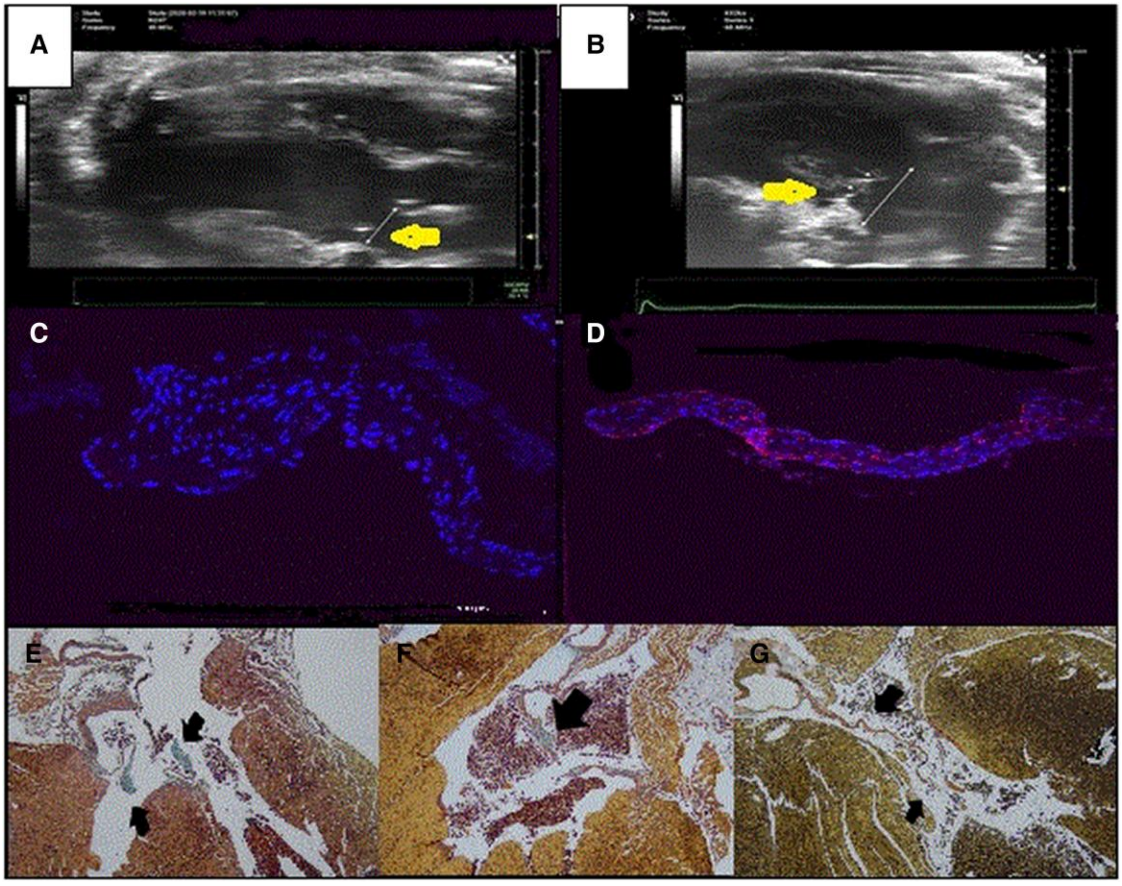

Figure 2 Valve phenotype of *LTBP2* deficiency. Echocardiograms of 6-month-old knockout (*A*) and wild type (*B*). The line delineates annular line. The arrow is pointing to the posterior leaflet. Mitral valve *LTBP2* immunofluorescence in a knockout mouse (*C*) and wild type (*D*). Notice the Cy5 colouring (red) of the wild-type valve that is lacking in the knockout. (*E–G*) Movat pentachrome straining of knockout, knockin, and wild-type mice, respectively. Black arrows are pointing at the leaflets. Notice the marked thickening and fibrosis with myxomatous changes of the valve leaflets in the knockout (black arrows) (*E*) and the widespread blue staining of mucinous substance (arrow) (*F*). The leaflets of the wild-type mice are thin and are not stained blue (*G*).

sections (*Table 3*). To understand if *LTBP2* deficiency affects ECM, we stained the leaflets for elastin. Knockout mice demonstrated significantly higher elastin deposition both qualitatively and quantitatively (57 322 μm per valve vs. 20 170 μm for KO and WT, respectively, $P = 0.000139$).

Echocardiogram

Seven out of nine KO animals showed leaflet prolapse compared with none of the eight in the control group ($P = 0.0011$). Knockin mice demonstrated a higher incidence of the phenotype as well, with six out of eight exhibiting it compared with none of eight in the control group ($P = 0.00123$) (refer to *Figure 2E and F*).

Quantitative polymerase chain reaction for *RUNX2* and periostin

Ample evidence suggests that the TGF-β–LTBP–fibrillin complex is important for both ECM integrity and appropriate TGF-β/cytokine signalling. Given that LTBPs are regulators of TGF-β signalling, we analysed the expression of three TGF-β target molecules in valve tissue RNA extracts: *RUNX2* (Runx family transcription factor 2), Periostin, and CTGF (a member of the connective tissue growth factor family).[29] Significant overexpression of both *Runx2* and Periostin was found in *LTBP2* KO valve tissue (*RUNX2* $P = 0.0144$ and Periostin $P = 0.001826$). There was no significant difference in CTGF expression.

Exploring eye phenotype

In vivo OCT imaging of the anterior chamber of the eye demonstrated a statistically significant increase in the depth of the anterior chamber in 12–14-month-old *LTBP2* KO mice when compared with age-matched control mice (746.3 ± 27.1 vs. 376.3 ± 4.6 μm in WT eyes, mean ± SEM, $P < 0.0001$; *Figure 3A*). Additionally, a substantial increase in the iridocorneal angle of the anterior chamber was identified ($50.5 \pm 1.2°$ vs. $35.6 \pm 1.1°$ in WT eyes, $P < 0.0001$; *Figure 3B*). Furthermore, from 12 months of age and on, *LTBP2* KO mice exhibited very poor dilation of the pupils in response to topical application of mydriatic drops. Measurements revealed a statistically significant reduction in pupil diameter following application of cyclopentolate and tropicamide dilating drops in mutant mice compared to age-matched control mice (1641.8 ± 153.1 μm vs. 2946.3 ± 90.5 μm in WT eyes, $P < 0.0001$; *Figure 3C*). The results obtained by *in vivo* OCT imaging correlated well with *ex vivo* histological findings of the eye (*Figure 3D*). In addition,

Table 3 The number of positive phenotypes among wild-type and mutated animals for myxomatous degeneration by histology (Movat column), valve prolapse by echocardiography, aortic diameter by echocardiography, and mitral valve leaflet area by histologic planimetry

Genotype	Movat staining	Echocardiogram	Aorta diameter	Heart weight/body weight	Anterior leaflet area (μm²)	Posterior leaflet area (μm²)
LTBP2 KO	7 (9)	7 (9)	2.0371000	0.006923935	128 757.496	39 687.838
LTBP2 WT	0 (7)	0 (8)	1.687500	0.007725334	48 082.63	26 858.38
P-value	0.00186	0.0011	0.000040	0.085314125	0.0034	0.026
LTBP2 KI	8 (8)	6 (8)	Not available	0.008103227	136 048.03	43 154.73
LTBP2 WT	0 (9)	0 (9)	Not available	0.008138468	48 082.63	26 858.38
P-value	0.00004	0.00123	Not available	0.972922022	0.006	0.009

The absolute number of animals, out of total (*n*), and the per cent are given in the bottom line. *P*-value is calculated by the χ^2 test.
KO, complete LTBP2 knockout; KI, homozygous for *LTBP2* V1506M mutation.

histological sections showed that in the eyes of mutant animals, there is displacement of the lens towards the posterior pole of the eye, significantly reducing vitreous chamber depth and bringing the lens in close approximation to the retina. The structural changes led to impairment of visual function. Visual acuity as measured using the optomotor response in adult (12–14 months old) mutant animals revealed a dramatic reduction in acuity compared with age-matched control mice (0.15 ± 0.1 cycles/degree vs. 0.39 ± 0.0 cycles/degree in WT eyes, $P < 0.05$; *Figure 3E*).

Discussion

Recently, Roselli *et al.*[10] described an association between *LTBP2* and MVP in a large GWAS. We identified a family with MVP with an *LTBP2* rs117800773 V1506M mutation that segregated with the trait with a high degree of penetrance (10 individuals out of 28). Our family has non-syndromic (isolated) type of MVP. Some of the family members have severe form of the disease. It seems that the disease severity is age dependent as MR severity as well as the need for surgical repair appears only in middle-aged individuals. Age-dependent progression of MVP phenotype was demonstrated before by Delling *et al.*[21] in the Framingham heart cohort.

The significant association of *LTBP2* with MVP in two distinct cohorts and using two different genetic approaches strongly supports its role as a causative gene for the disease. It is likely that the V1506M mutation has only minor effect on extracellular tissue integrity; therefore, penetrance occurs later in life and is not full.

We created two mouse models, the *LTBP2* KO and the *LTBP2* KI carrying the rs117800773 V1506M mutation. Both strains exhibited a high prevalence of MVP, as observed through echocardiography and histological analysis. Moreover, the KO animals displayed a significant aortic dilation. Furthermore, in contrast to WT mice, mutant mice lacking *LTBP2* exhibited posterior displacement of the lens leading to a significant increase in ACD and a wider iridocorneal angle. Our combined findings from both human and animal models substantiate the involvement of *LTBP2* in the development and progression of MVP, elucidating their potential role in the pathogenesis of the condition. These changes were related to changes in TGF-β signalling proteins, such as RUNX and periostin. Our KO model manifests a pronounced impact on myxomatous degeneration as seen both with Movat staining and increased elastin deposition. We therefore assume that LTBP2 plays a role in both ECM structure and TGF-β signalling. As expected and demonstrated before, *LTBP2* deficiency results in eye anterior chamber phenotype in mice. The KI effect suggests that the identified human mutation is pathogenic. However, the mutation may also be in linkage disequilibrium with another mutation in the gene in this family. Interestingly, not all mutated mice exhibited an MVP similar to humans, where penetrance is incomplete. This observation suggests that MVP is a progressive phenomenon and penetrance may be age dependent.[21]

The *LTBP2* gene, mapped to chromosome 14, is an isoform of the LTBP superfamily of ECM proteins. These are large, secreted glycoproteins structurally related to fibrillins. *LTBP2* is expressed abundantly and its expression is particularly strong in tissues enriched in microfibrils, such as the aorta, lung, heart, thyroid, ovary, and testis.[30,31] *LTBP2* is associated with ECM proteins, TGF-β, fibrillin, and elastin regulation pathways. However, the specific roles of *LTBP2* in ECM function are unknown. *LTBP2* is a unique member of the family as it is the only isoform that does not directly bind to latent TGF-β.[32] *LTBP2* not only colocalizes with fibrillin microfibrils, but its deposition is dependent on preformed fibres of fibrillin-1 (FBN1). *LTBP2* competes with *LTBP1* to bind to the same binding site in fibrillin-containing microfibrils, leading to the release of *LTBP1* from microfibrils,[19] and thus may indirectly negatively regulate the activation of TGF-β by releasing *LTBP1* from microfibrils. Indeed, deficiency of the long form of *LTBP1* in mice causes serious disruption of great vessels and cardiac valve development, resulting in perinatal death.[33–35] In our animal model, we demonstrated increased expression of TGF-β effector genes, *RUNX2* and periostin. These play an important role in cardiac development and are known regulators of ECM remodelling. *RUNX2* is a TGF-β and bone morphogenetic protein regulated gene required for epithelial mesenchymal transition. Periostin is a secreted fasciclin domain–containing protein, which is involved in both valve development and valvular heart disease.[30] Several studies demonstrated the importance of periostin in developing heart valves. Mice lacking periostin showed irregular matrix organization as periostin promotes cellular organization and differentiation of mesenchymal cells.[36,37] *RUNX2* is a regulator of endothelial mesenchymal transformation, a process important in normal valve development.[38]

The importance of fibrillin for valve structure was elucidated in the MFS. Marfan syndrome (MIM 154700) is a rare autosomal dominant hereditary disorder of connective tissue with prominent manifestations in the skeletal, ocular, and cardiovascular systems. The changes typically seen in the cardiovascular system are dilatation of the aorta and MVP. Marfan syndrome is caused by mutations in the gene for FBN1.[39–41] Fibrillin-1 assembles into microfibrils that serve a critical role in the maintenance of the structural integrity of the aortic wall, as well as the ciliary apparatus supporting the ocular lens. Hence, FBN1 mutations were initially thought to lead to tissue fragility, exclusively through

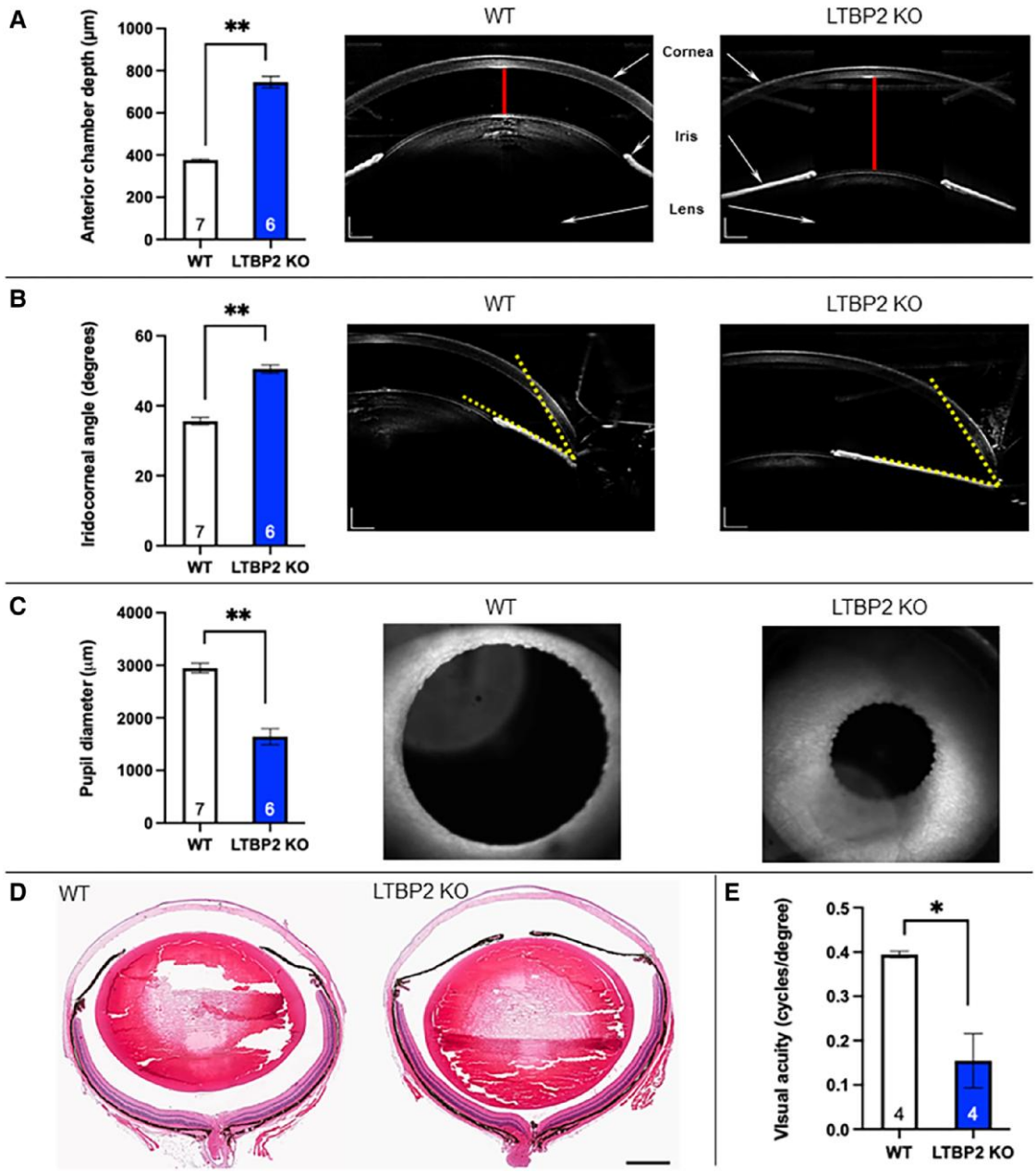

Figure 3 Ocular structure and visual function. Ocular structure and visual function in 12–14-month-old *LTBP2* knockout mice. Left bars represent wild-type mice, and right bars represent *LTBP2* knockout mice. Results are presented as mean ± SEM. Number of animals in each group is written within the corresponding bar. *$P < 0.05$; **$P < 0.0001$. (*A*) Comparison between wild-type and *LTBP2* knockout mouse eyes revealed a significant increase in the anterior chamber depth in mutant mice as measured using *in vivo* optical coherence tomography imaging of the anterior segment. Representative images from 12-month-old mice are shown to the right of the bar graph. Anterior chamber depth reflects the distance between the corneal endothelium and the anterior capsule of the lens and is marked by red lines. Scale bars, 240 μm. (*B*) Knockout of the *LTBP2* gene also led to significant enlargement of the iridocorneal angle. Representative images of iridocorneal angle (marked by yellow dotted lines) in 12-month wild-type and *LTBP2* knockout mice. (*C*) From 12 months of age and on, *LTBP2* knockout mice exhibited very poor dilation of the pupils in response to topical application of mydriatic drops. Measurements revealed a statistically significant reduction in pharmacologically dilated pupil diameter in mutant mice compared with age-matched wild-type mice. Representative images of eyes of 12-month-old mice captured in infra-red mode are presented to the right of the graph. (*D*) Representative images of eye sections from 12-month-old mice, taken through the central cornea and optic nerve and stained with haematoxylin and eosin, align with our *in vivo* optical coherence tomography findings. Mutant eyes show a deeper anterior chamber caused by posterior subluxation of the lens accompanied by an increased iridocorneal angle, reduced depth of the vitreous cavity, and a narrow pupil. Scale bar, 500 μm. (*E*) Visual acuity as measured using the optomotor response revealed a significant reduction in *LTBP2* knockout mice compared with wild-type mice.

disintegration and fragmentation of the connective tissue fibres. A revolutionary shift in thinking about the mechanisms of MFS occurred by studying lung disease in FBN1-deficient mice. In the lungs of developing mice, increased levels of free TGF-β in addition to the downstream effectors of TGF-β signalling (pSMAD2/3) coincided with primary failure of distal alveolar septation. *In vivo* TGF-β antagonism using neutralizing anti-TGF-β antibody prevented the lung phenotype. Similarly, involvement of dysregulated TGF-β signalling in the aetiology of MFS was subsequently established by Ng *et al.*[28] for the myopathy, MVP, and the aortic aneurysmal phenotype. As stated above, TGF-β interacts with fibrillin in the ECM through the LAP complex. Because of this interaction, TGF-β bioavailability is meticulously controlled by cytokine sequestration into the ECM LAP complex. Fibrillin-1 deficiency, due to FBN1 mutations, impairs ECM targeting of the LAP, resulting in an unrestrained release of TGF-β ligands.[41] Evidence suggests that the TGF-β–LTBP–fibrillin complex is important for both ECM integrity and appropriate TGF-β/cytokine signalling. Mutations in this pathway were shown to generate MVP. Our study points to the importance of TGF-β–LTBP–fibrillin complex in normal valve physiology and its relation to pathogenesis of MVP. This pathway may present an opportunity for pharmacological targeting to modify disease progression, as suggested by the study of Ng *et al.*[28]

Our data recapitulate finding by others[31,42,43] by demonstrating lens dislocation and reduced VA. The reduction in VA observed in *LTBP2* KO mice can probably be attributed to the dislocation of the lens, a condition known as ectopia lentis. This parallels the human clinical manifestation of ectopia lentis, when progressive subluxation or complete dislocation of the lens can cause a high degree of myopia and reduction in VA varies with the type and degree of dislocation. The lens dislocation in *LTBP2* KO mice likely disrupts the normal refraction of light onto the retina, impairing the sharpness and clarity of the visual image. Further investigation into the structural and functional integrity of the ocular components in *LTBP2* KO mice could elucidate the mechanistic pathways linking *LTBP2* deficiency to lens stability and VA.

Our study has several limitations: as of the writing of this article, we have found only one family carrying the current mutation. This may limit the generalizability of our findings. However, the recent GWAS cited above that found a hit adjacent to the *LTBP2* gene[10] provides confirmation from another cohort. Antonutti *et al.*[44] described that *LTBP2* mutations are associated with spontaneous coronary dissection. Morlino *et al.*[45] has described Marfan-like features in Roma/Gypsy subjects with the *LTBP2* homozygous p.R299X variant. The latter two further support *LTBP2* role in normal ECM stability in various tissues and that the phenotype may expand to other organs. Our initial data support changes in elastin deposition. The exact role of *LTBP2* in the pathogenesis of MVP remains unclear. Future work will seek to identify and explore the specific molecular mechanisms that link *LTBP2* and ECM homeostasis signalling pathways. We hypothesize that *LTBP2* has a lifelong role in homeostasis and maintenance of the elasticity of the tissues. It may serve as potential therapeutic target in the future and a biomarker to related cardiovascular phenotypes, such as MVP.

Conclusions

A recent large GWAS found an association between *LTBP2* and MVP.[10] We provide data on a pedigree with *LTBP2* mutation linked to the trait. Our animal model data provide evidence for the important role of *LTBP2* in normal mitral function and structure. Sequence variations and mutations in this gene cause myxomatous valve degeneration. This model may serve in the future for studies aimed at better understanding myxomatous degeneration pathogenesis and to test potential therapies.

Lead author biography

Shoshi Shpitzen is a PhD candidate in cardiovascular biology at the Hebrew University Medical School and an MSc graduate in genetics from the same institution. Her research focuses on heart genetic conditions, including connective tissue disorders, lipid disorders, and cardiomyopathies. She has expertise in both human genetics and animal modelling of these diseases.

Data availability

The data underlying this article are available in the article and in its online supplementary material.

Supplementary material

Supplementary material is available at *European Heart Journal Open* online.

Acknowledgements

We thank Dr Gerhad Sengle for providing *LTBP2* antibodies for valve immunostaining.

Funding

The paper was supported by BSF grant 2017265 and Hadassah Medical Center bridge grant in 2021.

Conflict of interest: None declared.

References

1. Freed LA, Levy D, Levine RA, Larson MG, Evans JC, Fuller DL, Lehman B, Benjamin EJ. Prevalence and clinical outcome of mitral-valve prolapse. *N Engl J Med* 1999;**341**:1–7.
2. Mitchell C, Rahko PS, Blauwet LA, Canaday B, Finstuen JA, Foster MC, Horton K, Ogunyankin KO, Palma RA, Velazquez EJ. Guidelines for performing a comprehensive transthoracic echocardiographic examination in adults: recommendations from the American Society of Echocardiography. *J Am Soc Echocardiogr* 2019;**32**:1–64.
3. Levine Robert A, Durst R. Mitral valve prolapse: a deeper look. *JACC Cardiovasc Imaging* 2008;**1**:304–306.
4. Levine RA, Hagége AA, Judge DP, Padala M, Dal-Bianco JP, Aikawa E, Beaudoin J, Bischoff J, Bouatia-Naji N, Bruneval P, Butcher JT, Carpentier A, Chaput M, Chester AH, Clusel C, Delling FN, Dietz HC, Dina C, Durst R, Fernandez-Friera L, Handschumacher MD, Jensen MO, Jeunemaitre XP, Le Marec H, Le Tourneau T, Markwald RR, Mérot J, Messas E, Milan DP, Neri T, Norris RA, Peal D, Perrocheau M, Probst V, Pucéat M, Rosenthal N, Solis J, Schott JJ, Schwammenthal E, Slaugenhaupt SA, Song JK, Yacoub MH; Leducq Mitral Transatlantic Network. Mitral valve disease—morphology and mechanisms. *Nat Rev Cardiol* 2015;**12**:689–710.
5. Guicciardi NA, De Bonis M, Di Resta C, Ascione G, Alfieri O, Maisano F, Vergara P. Genetic background of mitral valve prolapse. *Rev Cardiovasc Med* 2022;**23**:96.
6. Sriram CS, Syed FF, Ferguson ME, Johnson JN, Enriquez-Sarano M, Cetta F, Cannon BC, Asirvatham SJ, Ackerman MJ. Malignant bileaflet mitral valve prolapse syndrome in patients with otherwise idiopathic out-of-hospital cardiac arrest. *J Am Coll Cardiol* 2013;**62**:222–230.
7. Essayagh B, Sabbag A, Antoine C, Benfari G, Yang LT, Maalouf J, Asirvatham S, Michelena H, Enriquez-Sarano M. Presentation and outcome of arrhythmic mitral valve prolapse. *J Am Coll Cardiol* 2020;**76**:637–649.
8. Levy S, Sharaf Dabbagh G, Giudicessi JR, Haqqani H, Khanji MY, Obeng-Gyimah E, Betts MN, Ricci F, Asatryan B, Bouatia-Naji N, Nazarian S, Chahal CAA. Genetic mechanisms underlying arrhythmogenic mitral valve prolapse: current and future perspectives. *Heart Rhythm O2* 2023;**4**:581–591.
9. Parwani P, Avierinos J-F, Levine RA, Delling FN. Mitral valve prolapse: multimodality imaging and genetic insights. *Prog Cardiovasc Dis* 2017;**60**:361–369.

10. Roselli C, Yu M, Nauffal V, Georges A, Yang Q, Love K, Weng LC, Delling FN, Maurya SR, Schrolkamp M, Tfelt-Hansen J, Hagège A, Jeunemaitre X, Debette S, Amouyel P, Guan W, Muehlschlegel JD, Body SC, Shah S, Samad Z, Kyryachenko S, Haynes C, Rienstra M, Le Tourneau T, Probst V, Roussel R, Wijdh-Den Hamer IJ, Siland JE, Knowlton KU, Jacques Schott J, Levine RA, Benjamin EJ, Vasan RS, Horne BD, Muhlestein JB, Benfari G, Enriquez-Sarano M, Natale A, Mohanty S, Trivedi C, Shoemaker MB, Yoneda ZT, Wells QS, Baker MT, Farber-Eger E, Michelena HI, Lundby A, Norris RA, Slaugenhaupt SA, Dina C, Lubitz SA, Bouatia-Naji N, Ellinor PT, Milan DJ. Genome-wide association study reveals novel genetic loci: a new polygenic risk score for mitral valve prolapse. *Eur Heart J* 2022;**43**:1668–1680.
11. Nishiura K, Yokokawa T, Misaka T, Ichimura S, Tomita Y, Miura S, Shimizu T, Sato T, Kaneshiro T, Oikawa M, Kobayashi A, Yoshihisa A, Takeishi Y. Prognostic role of circulating LTBP-2 in patients with dilated cardiomyopathy: a novel biomarker reflecting extracellular matrix LTBP-2 accumulation. *Can J Cardiol* 2023;**39**:1436–1445.
12. Levine RA, Handschumacher MD, Sanfilippo AJ, Hagege AA, Harrigan P, Marshall JE, Weyman AE. Three-dimensional echocardiographic reconstruction of the mitral valve, with implications for the diagnosis of mitral valve prolapse. *Circulation* 1989;**80**:589–598.
13. Zoghbi WA, Adams D, Bonow RO, Enriquez-Sarano M, Foster E, Grayburn PA, Hahn RT, Han Y, Hung J, Lang RM, Little SH, Shah DJ, Shernan S, Thavendiranathan P, Thomas JD, Weissman NJ. Recommendations for noninvasive evaluation of native valvular regurgitation: a report from the American Society of Echocardiography developed in collaboration with the Society for Cardiovascular Magnetic Resonance. *J Am Soc Echocardiogr* 2017;**30**:303–371.
14. Dahary D, Golan Y, Mazor Y, Zelig O, Barshir R, Twik M, Iny Stein T, Rosner G, Kariv R, Chen F, Zhang Q, Shen Y, Safran M, Lancet D, Fishilevich S. Genome analysis and knowledge-driven variant interpretation with TGex. *BMC Med Genomics* 2019;**12**:200.
15. Hsu PD, Scott DA, Weinstein JA, Ran FA, Konermann S, Agarwala V, Li Y, Fine EJ, Wu X, Shalem O, Cradick TJ, Marraffini LA, Bao G, Zhang F. DNA targeting specificity of RNA-guided Cas9 nucleases. *Nat Biotechnol* 2013;**31**:827–832.
16. Doench JG, Fusi N, Sullender M, Hegde M, Vaimberg EW, Donovan KF, Smith I, Tothova Z, Wilen C, Orchard R, Virgin HW, Listgarten J, Root DE. Optimized sgRNA design to maximize activity and minimize off-target effects of CRISPR-Cas9. *Nat Biotechnol* 2016;**34**:184–191.
17. Benchling, Could based plabform for biotech R&D. www.benchling.com. 2022.
18. Xu H, Xiao T, Chen C-H, Li W, Meyer CA, Wu Q, Wu D, Cong L, Zhang F, Liu JS, Brown M, Liu XS. Sequence determinants of improved CRISPR sgRNA design. *Genome Res* 2015;**25**:1147–1157.
19. Concordet JP, Haeussler M. CRISPOR: intuitive guide selection for CRISPR/Cas9 genome editing experiments and screens. *Nucleic Acids Res* 2018;**46**:W242–W245.
20. Gertsenstein M, Nutter LMJ. Production of knockout mouse lines with Cas9. *Methods* 2021;**191**:32–43.
21. Delling FN, Gona P, Larson MG, Lehman B, Manning WJ, Levine RA, Benjamin EJ, Vasan RS. Mild expression of mitral valve prolapse in the Framingham offspring: expanding the phenotypic spectrum. *J Am Soc Echocardiogr* 2014;**27**:17–23.
22. Durst R, Sauls K, Peal DS, deVlaming A, Toomer K, Leyne M, Salani M, Talkowski ME, Brand H, Perrocheau M, Simpson C, Jett C, Stone MR, Charles F, Chiang C, Lynch SN, Bouatia-Naji N, Delling FN, Freed LA, Tribouilloy C, Le Tourneau T, LeMarec H, Fernandez-Friera L, Solis J, Trujillano D, Ossowski S, Estivill X, Dina C, Bruneval P, Chester A, Schott JJ, Irvine KD, Mao Y, Wessels A, Motiwala T, Puceat M, Tsukasaki Y, Menick DR, Kasiganesan H, Nie X, Broome AM, Williams K, Johnson A, Markwald RR, Jeunemaitre X, Hagege A, Levine RA, Milan DJ, Norris RA, Slaugenhaupt SA. Mutations in DCHS1 cause mitral valve prolapse. *Nature* 2015;**525**:109–113.
23. Matsevich C, Gopalakrishnan P, Obolensky A, Banin E, Sharon D, Beryozkin A. Retinal structure and function in a knock-in mouse model for the FAM161A-p.Arg523 * human nonsense pathogenic variant. *Ophthalmol Sci* 2023;**3**:100229.
24. Loeys BL, Dietz HC, Braverman AC, Callewaert BL, Backer JD, Devereux RB, Hilhorst-Hofstee Y, Jondeau G, Faivre L, Milewicz DM, Pyeritz RE, Sponseller PD, Wordsworth P, De Paepe AM. The revised Ghent nosology for the Marfan syndrome. *J Med Genet* 2010;**47**:476–485.
25. MacCarrick G, Black JH III, Bowdin S, El-Hamamsy I, Frischmeyer-Guerrerio PA, Guerrerio AL, Sponseller PD, Loeys B, Dietz HC III. Loeys-Dietz syndrome: a primer for diagnosis and management. *Genet Med* 2014;**16**:576–587.
26. Malfait F, Francomano C, Byers P, Belmont J, Berglund B, Black J, Bloom L, Bowen JM, Brady AF, Burrows NP, Castori M, Cohen H, Colombi M, Demirdas S, De Backer J, De Paepe A, Fournel-Gigleux S, Frank M, Ghali N, Giunta C, Grahame R, Hakim A, Jeunemaitre X, Johnson D, Juul-Kristensen B, Kapferer-Seebacher I, Kazkaz H, Kosho T, Lavallee ME, Levy H, Mendoza-Londono R, Pepin M, Pope FM, Reinstein E, Robert L, Rohrbach M, Sanders L, Sobey GJ, Van Damme T, Vandersteen A, van Mourik C, Voermans N, Wheeldon N, Zschocke J, Tinkle B. The 2017 international classification of the Ehlers–Danlos syndromes. *Am J Med Genet C Semin Med Genet* 2017;**175**:8–26.
27. ClinVar - NCBI. rs117800773. https://www.ncbi.nlm.nih.gov/clinvar/variation/314272/?oq=rs117800773&m=NM_000428.3(LTBP2):c.4516G%3EA%20(p.Val1506Met). 2024.
28. Ng CM, Cheng A, Myers LA, Martinez-Murillo F, Jie C, Bedja D, Gabrielson KL, Hausladen JM, Mecham RP, Judge DP, Dietz HC. TGF-beta-dependent pathogenesis of mitral valve prolapse in a mouse model of Marfan syndrome. *J Clin Invest* 2004;**114**:1586–1592.
29. Doetschman T, Barnett JV, Runyan RB, Camenisch TD, Heimark RL, Granzier HL, Conway SJ, Azhar M. Transforming growth factor beta signaling in adult cardiovascular diseases and repair. *Cell Tissue Res* 2012;**347**:203–223.
30. Genecard suite. https://www.genecards.org/cgi-bin/carddisp.pl?gene=LTBP2&keywords=ltbp2#expression.
31. Shi Y, Jones W, Beatty W, Tan Q, Mecham RP, Kumra H, Reinhardt DP, Gibson MA, Reilly MA, Rodriguez J, Bassnett S. Latent-transforming growth factor beta-binding protein-2 (LTBP-2) is required for longevity but not for development of zonular fibers. *Matrix Biol* 2021;**95**:15–31.
32. Saharinen J, Keski-Oja J. Specific sequence motif of 8-Cys repeats of TGF-beta binding proteins, LTBPs, creates a hydrophobic interaction surface for binding of small latent TGF-beta. *Mol Biol Cell* 2000;**11**:2691–2704.
33. Todorovic V, Finnegan E, Freyer L, Zilberberg L, Ota M, Rifkin DB. Long form of latent TGF-beta binding protein 1 (Ltbp1L) regulates cardiac valve development. *Dev Dyn* 2011;**240**:176–187.
34. Todorovic V, Frendewey D, Gutstein DE, Chen Y, Freyer L, Finnegan E, Liu F, Murphy A, Valenzuela D, Yancopoulos G, Rifkin DB. Long form of latent TGF-beta binding protein 1 (Ltbp1L) is essential for cardiac outflow tract septation and remodeling. *Development* 2007;**134**:3723–3732.
35. Drews F, Knobel S, Moser M, Muhlack KG, Mohren S, Stoll C, Bosio A, Gressner AM, Weiskirchen R. Disruption of the latent transforming growth factor-beta binding protein-1 gene causes alteration in facial structure and influences TGF-beta bioavailability. *Biochim Biophys Acta* 2008;**1783**:34–48.
36. Norris RA, Moreno-Rodriguez RA, Sugi Y, Hoffman S, Amos J, Hart MM, Potts JD, Goodwin RL, Markwald RR. Periostin regulates atrioventricular valve maturation. *Dev Biol* 2008;**316**:200–213.
37. Qiao B, Liu X, Wang B, Wei S. The role of periostin in cardiac fibrosis. *Heart Fail Rev* 2023;**29**:191–206.
38. Tavares ALP, Brown JA, Ulrich EC, Dvorak K, Runyan RB. Runx2-I is an early regulator of epithelial-mesenchymal cell transition in the chick embryo. *Dev Dyn* 2018;**247**:542–554.
39. Dietz HC, Cutting GR, Pyeritz RE, Maslen CL, Sakai LY, Corson GM, Puffenberger EG, Hamosh A, Nanthakumar EJ, Curristin SM, Stetten G, Meyers DA, Francomano CA. Marfan syndrome caused by a recurrent de novo missense mutation in the fibrillin gene. *Nature* 1991;**352**:337–339.
40. Robinson PN, Arteaga-Solis E, Baldock C, Collod-Béroud G, Booms P, De Paepe A, Dietz HC, Guo G, Handford PA, Judge DP, Kielty CM, Loeys B, Milewicz DM, Ney A, Ramirez F, Reinhardt DP, Tiedemann K, Whiteman P, Godfrey M. The molecular genetics of Marfan syndrome and related disorders. *J Med Genet* 2006;**43**:769–787.
41. Verstraeten A, Alaerts M, Van Laer L, Loeys B. Marfan syndrome and related disorders: 25 years of gene discovery. *Hum Mutat* 2016;**37**:524–531.
42. Narooie-Nejad M, Paylakhi SH, Shojaee S, Fazlali Z, Rezaei Kanavi M, Nilforushan N, Yazdani S, Babrzadeh F, Suri F, Ronaghi M, Elahi E, Paisán-Ruiz C. Loss of function mutations in the gene encoding latent transforming growth factor beta binding protein 2, LTBP2, cause primary congenital glaucoma. *Hum Mol Genet* 2009;**18**:3969–3977.
43. Inoue T, Ohbayashi T, Fujikawa Y, Yoshida H, Akama TO, Noda K, Horiguchi M, Kameyama K, Hata Y, Takahashi K, Kusumoto K, Nakamura T. Latent TGF-beta binding protein-2 is essential for the development of ciliary zonule microfibrils. *Hum Mol Genet* 2014;**23**:5672–5682.
44. Antonutti M, Baldan F, Lanera C, Spedicato L, Zanuttini D, Bisceglia T, Favaretto E, Poli S, Tioni C, Sut D, Gregori D, Damante G, Proclemer A. Spontaneous coronary artery dissection: role of prognostic markers and relationship with genetic analysis. *Int J Cardiol* 2021;**326**:19–29.
45. Morlino S, Alesi V, Calì F, Lepri FR, Secinaro A, Grammatico P, Novelli A, Drago F, Castori M, Baban A. LTBP2-related "Marfan-like" phenotype in two Roma/Gypsy subjects with the LTBP2 homozygous p.R299X variant. *Am J Med Genet A* 2019;**179**:104–112.